

Properties of liquid silicon observed by time-resolved x-ray absorption spectroscopy

S. L. Johnson¹, P. A. Heimann², A. M. Lindenberg¹, H. O. Jeschke³,
M. E. Garcia³, Z. Chang⁴, R. W. Lee⁵, J. J. Rehr⁶, and R. W. Falcone^{1,7}

¹*Department of Physics, University of California, Berkeley, CA 94720, USA*

²*Advanced Light Source, Lawrence Berkeley National Laboratory, Berkeley, CA 94720, USA*

³*Institut für Theoretische Physik, Freie Universität Berlin,
Arnimallee 14, 14195 Berlin, Germany*

⁴*Department of Physics, Kansas State University, Manhattan, KS 66506, USA*

⁵*Lawrence Livermore National Laboratory, Livermore, CA 94551, USA*

⁶*Department of Physics, University of Washington, Seattle, WA 98195, USA*

⁷*Center for Beam Physics, Lawrence Berkeley
National Laboratory, Berkeley, CA 94720, USA*

(Dated: March 25, 2003)

Abstract

Time-resolved x-ray spectroscopy at the Si L -edges is used to probe the electronic structure of an amorphous Si foil as it melts following absorption of an ultrafast laser pulse. Picosecond temporal resolution allows observation of the transient liquid phase before vaporization and before the liquid breaks up into droplets. The melting causes large changes in the spectrum that match the predictions of molecular dynamics and ab-initio x-ray absorption codes.

PACS numbers: 78.70.Dm,64.70.Dv,61.20.Ja,71.22.+i

The melting of solid, covalently bonded semiconductors into metallic liquids has attracted considerable attention due to both the technological importance of semiconductor processing and the peculiar nature of the liquids, which typically have coordination numbers of 6–7, in contrast to most liquid metals with coordination numbers of 10–12 [1–3]. This lower coordination number is presumably due to a persistence of covalent bonding in the melt. Molecular dynamics simulations of molten Si have suggested that approximately 30% of the bonding in liquid Si is covalent and that the bonding in the melt is a highly dynamic phenomenon, with bonds rapidly forming and breaking on a time scale of 20 fs [4]. Although x-ray and neutron diffraction experiments have accurately characterized the atomic structure of liquid Si [5, 6], experimental investigation of the electronic structure is incomplete and may yield further insights.

X-ray spectroscopy is a powerful experimental means for investigating electronic structure. The high temperature and volatile nature of liquid Si are, however, not compatible with spectroscopic methods used for static samples. The introduction of time resolution corrects this deficiency. In our experiment, a short laser pulse (150 fs duration, 800 nm wavelength) rapidly heats and melts a thin amorphous Si foil, producing a sheet of liquid that persists while x-rays probe absorption through the sample before the liquid vaporizes or breaks up into droplets. The resulting spectrum offers information on both the electronic structure via x-ray absorption near-edge spectroscopy (XANES) and the related atomic structure via extended x-ray absorption fine structure (EXAFS) of the transient liquid. Previous time-resolved x-ray studies of laser-melted Si using nanosecond laser pulses have demonstrated large changes in the vicinity of the Si *L*-edges [7, 8], but relatively coarse temporal and spectral resolution prevented quantitative conclusions.

Our measurements employ picosecond resolution to study laser-heated amorphous Si foils. Fig. 1 shows a sketch of relevant aspects of the setup at beamline 5.3.1 of the Advanced Light Source (ALS). A broad spectrum of pulsed soft x-ray light from a synchrotron bend magnet is focused by a grazing incidence toroidal mirror to a 300 μm diameter spot on the foil. Before reaching the foil, the beam reflects from a pair of flat carbon-coated mirrors that serve as a low-pass photon energy filter, with the energy cutoff set by both the carbon *K*-edge at 285 eV and the incidence angle θ of x-rays on the mirrors. The x-rays then strike the foil in the center of a 400 μm diameter laser-heated region. After passing through the foil, the x-rays enter a spectrograph that uses a varied-line-spaced grating to create

an energetically dispersed flat field image of the x-ray focus. The spectrograph diffracts the transmitted x-rays into a spectrum ranging from 85 eV to 300 eV with a resolution of approximately 1 eV near the Si $L_{II,III}$ edge at 100 eV. Proper adjustment of the angle θ of the carbon-coated mirrors suppresses higher-order grating reflections for a particular region of the spectrum, necessary because of the wide range of x-ray photon energies produced by the bend magnet.

Depending on the desired time resolution of the experiment, one of two types of detectors measure the resulting soft x-ray spectrum. For a resolution of about 70 ps, we use a gated set of imaging microchannel plates coupled to a phosphor screen and CCD camera. The gate width of the plates is 20 ns, sufficient to isolate a single x-ray pulse from the ALS filling pattern. By adjusting the relative timing of the laser and x-ray pulses, we obtain the spectrum as a function of time after excitation. The time resolution of this “pump-probe” technique is determined by the width of the x-ray pulse. For better resolution we employ an ultrafast x-ray streak camera to observe changes in intensity within the x-ray pulse length [9]. This instrument can record changes in the x-ray transmission spectrum faster than 1 ps within a single x-ray pulse at the cost of some experimental complexity and decreased quantum efficiency.

Representative data using the pump-probe technique are shown in Fig. 2 for a 500 Å foil with an incident laser fluence of 0.7 J/cm². The dashed curve shows the absorption spectrum before excitation. This spectrum of the unheated foil agrees with previous measurements on solid amorphous Si, allowing for a 30% error in the assumed areal density of the foils [10, 11]. The large edge at 100 eV is a superposition of the L_{II} and L_{III} spin-orbit split edges, which are not separately distinguishable due to the resolution of the spectrometer. At 150 eV the smaller L_I edge appears. Energies beyond approximately 280 eV were inaccessible due to absorption above the K -edge of carbon in the optical path.

The solid line in Fig. 2 shows the absorption spectrum 100 ps after laser excitation. The melting induced by the laser causes a dramatic effect at the $L_{II,III}$ edge; the magnitude of the edge is reduced by approximately 50%, and the edge is broadened to 2 eV. In addition the near-edge features of the $L_{II,III}$ edge are modified, the L_I edge is shifted to lower energies by 1.6 ± 0.2 eV, and the small $L_{II,III}$ EXAFS oscillations beyond the L_I edge disappear[28]. These features do not change significantly for longer pump-probe delays until about 10 ns after excitation. At this time, the overall transmission of the foil begins to

increase, suggesting that material is starting to leave the probed region. This observation is consistent with experimental and theoretical work on femtosecond laser ablation which suggest that the hydrodynamic evolution of the laser-melted foil results in an expanding 1-D liquid bubble with approximately constant temperature and density that persists for several nanoseconds [12, 13].

Measurements of the dependence of incident laser fluence on the near-threshold region of the $L_{II,III}$ edge show that the observed absorption changes take effect at approximately 0.1 J/cm^2 , and the changes reach a fluence-independent saturation level above 0.3 J/cm^2 . This threshold value is consistent with previous measurements of the threshold fluence for femtosecond melting in bulk Si [14], and the observed saturation at higher fluence suggests that under these conditions the probed region of the foil is completely melted. At the fluence of 0.7 J/cm^2 where all other reported measurements have been performed, transreflectance measurements using an integrating sphere show that 40% of the laser pulse energy is absorbed in the foil. If this energy is uniformly distributed over the thickness of the foil, a simple calculation using commonly accepted values of the latent heat of melting and the heat capacity of solid and liquid Si near the melting point suggests that the resultant liquid is highly superheated, with a calculated temperature of 25,000 K. This temperature is an overestimate, since we expect that the heat capacity will increase dramatically as the liquid approaches the critical temperature of Si near 5000 K because much of the energy at these temperatures is used to break strong interatomic bonds [15]. Also, adiabatic expansion of the foil will act to cool the liquid on a time scale set by the thickness of the foil divided by the sound speed, approximately 100 ps. Thus, the temperature of the foil after laser excitation is probably less than 5000 K. The thermal energy density in the foil is, however, high enough to eventually create a Si vapor at a temperature of approximately 3500 K, setting a lower bound on the expected temperature of the transient liquid. The temperature of the probed liquid Si is therefore likely to fall in the range of 3500–5000 K.

To achieve higher time resolution of the changes in the $L_{II,III}$ edge, we employed the streak camera detector to measure the transmission spectrum of a 1000 \AA foil with 5 ps resolution. To obtain better statistics for the dynamics of the edge drop, we integrated the signal over a 5 eV energy range above the edge. Fig. 3 shows this integrated post-edge absorption as a function of time after laser excitation. The absorption drop is instantaneous within the camera resolution. Further, the magnitude of the drop agrees with that observed

in pump-probe measurements on 1000 Å foils (a smaller effect than that observed in 500 Å foils, suggesting that the thicker foils are only partly melted even at 0.7 J/cm²)[29]. These observations are consistent with ultrafast optical measurements, where a transition from the solid to a high reflectivity, electronically disordered phase occurs on a time scale of 300 fs [14, 16].

To obtain models for comparison with the x-ray absorption data, we employed molecular dynamics (MD) simulations to calculate atomic structure and then used the ab-initio x-ray absorption code FEFF 8.1 [17] to calculate the photoabsorption spectra from this structure. We performed the MD simulations on a block of 216 atoms initially in a crystalline configuration, with periodic boundary conditions in a fixed volume supercell. The system (atoms + electrons) was heated by a laser pulse, as described in ref. [18, 19], and then permitted to equilibrate for several picoseconds to 3100 K, a temperature somewhat below the rough estimates developed above. The simulations used a tight-binding Hamiltonian with parameters from ref. [20]. The pair correlation function of the final state agrees with the results of x-ray diffraction measurements on liquid Si near the melting temperature [5, 6].

The FEFF calculations of the x-ray absorption spectra presented here use an initial state approximation. We also calculated the spectra using a fully statically screened core hole, but we found that this yields a poorer match to experiment for the near-edge structure of the solid Si $L_{II,III}$ edge in the range of 10–50 eV past the edge threshold, and it has little qualitative impact on the spectrum closer to the edges [30]. This static screening model neglects local field effects which tend to cancel the core-hole potential. This cancellation phenomenon is a particularly strong effect in the L edges of materials with low- d occupation [21, 22]. The dynamic screening model discussed in ref. [22] should provide better results, but for the present work the initial state approximation (assuming complete cancellation of the core-hole potential and local field effects) appears adequate.

To extract absorption spectra from the simulated liquid structure, we ran FEFF on each of approximately 50 randomly selected atoms as x-ray absorbers. The code calculated the spectrum of each absorber using a cluster of radius 6.1 Å encompassing about 30 atoms. We then averaged together the individual spectra to compare with experiment. We performed similar calculations on the spectrum of the initial solid using a published model structure of amorphous solid Si [23].

Fig. 4 shows a comparison of the model results for the near-edge structure of the $L_{II,III}$

edge for both the initial solid and the liquid. For energies above 110 eV, the model calculations are close to experiment. The prominent feature in this energy range is a broad absorption maximum near 125 eV. The model shows a -4 eV shift in this feature on melting that is consistent with the experiment[31]. This energy shift and the associated reduction of the peak on melting are consequences of the structural changes reflected by the pair correlation function, namely an increase in disorder and an expansion of the nearest-neighbor distance by 0.15 ± 0.07 Å (compared against the 2.35 Å nearest neighbor spacing in solid Si). The onset of short-range disorder upon melting also suppresses the EXAFS structure at higher energies via a reduction in the Debye-Waller factor $e^{-2\sigma^2 k^2}$, where σ is the variance of the bond length distribution and k is the photoelectron wavenumber, larger than 4 Å⁻¹ for photon energies above 160 eV. Melting causes a large increase in σ from 0.065 Å at room temperature [24] to 0.25 Å, pushing down the EXAFS oscillation amplitude to well below the noise level. The observed and calculated shape of the spectrum at these energies are thus consistent with previously measured structural properties of liquid Si.

Closer to the edge threshold, the agreement is mostly qualitative, possibly due to the neglect of non-spherical components of the electron potential in FEFF [25]. The MD calculations show that the melting of Si causes a “flattening” of the density of states (DOS) near the Fermi level and a collapse of the semiconductor band gap. This change in the DOS manifests itself in the spectra as a reduction in the near-threshold absorption, evident in both the model spectra and the experimental data. The inset of Fig. 4 shows a plot of the 3s-projected unoccupied DOS from the MD calculations. A comparison of these curves to the observed near-threshold absorption is favorable to within a few eV of the edge, reflecting the large drop in absorption immediately above the edge. This agreement persists even though such a comparison ignores both contributions to the edge structure from other unoccupied states permitted by selection rules and the potentially important core hole effects that have been shown in crystalline Si to shift the $L_{II,III}$ edge by -1 eV [26]. The 2 eV edge broadening observed for the liquid $L_{II,III}$ edge but not reproduced by the modeling may be the result of simultaneously probing a wide range of liquid densities in the experiment. By running FEFF on uniform dilations and contractions of the liquid model structure, we estimated that a 30% distribution of densities around the density of the liquid model is sufficient to cause a 2 eV edge broadening due to shifts of the Fermi level with respect to the 2p core levels. This wide density distribution also broadens and reduces by 5% the absorption maximum

near 125 eV, bringing it closer to the experimental observations. Such a large variation in density might be explained by non-uniformities of energy deposition along the 300 μm x-ray spot size, or perhaps by the large local density fluctuations expected in liquids when pushed to temperatures near the critical point [15, 27]. Extending the MD simulations to higher temperatures could provide further insight into this issue.

Calculations on the L_I edge are shown in Fig. 5. Although the models for both the solid and liquid forms of Si show edge thresholds that differ from experimental values by about 5 eV, the model spectra do show an edge shift of approximately -1.2 eV from the solid to the liquid due to band gap collapse, close to the observed -1.6 ± 0.2 eV shift. The unoccupied 3p-DOS plotted in the inset of Fig. 5 shows a similar shift of -1.1 eV. Like the changes in the near-edge structure of the $L_{II,III}$ edge, the L_I edge shift appears to be at least partly due to collapse of the semiconductor band gap on melting. Note that, compared to the $L_{II,III}$ edge, the L_I edge is less sensitive to broadening effects caused by density variations because of its already large lifetime and instrumental broadening.

By comparing the entirety of the model calculations with the data, we conclude that the high-temperature liquid Si produced by the laser is a structurally disordered metal with a nearest neighbor distance in agreement with that previously measured for liquid Si near the melting temperature. Although agreement between experiment and the model is already quite good, further improvement might result from a more sophisticated treatment of final-state effects and by extending the MD simulations to even higher temperatures to explore the effects of near-critical local density fluctuations. This work has demonstrated a new technique for quantitatively studying volatile, high-temperature, near solid-density materials using x-ray absorption spectroscopy. The combination of short-pulse laser sources and temporally resolved x-ray absorption spectroscopy offers the potential to explore the electronic structure of materials under temperatures and pressures inaccessible by other experimental means.

The authors would like to acknowledge A. Ng for fruitful discussions and Th. Missalla for contributions to an early phase of this experiment. This work was supported by the Department of Energy, through the Office of Science and through the High-Energy-Density Grants Program, and the Institute for Laser Science and Applications at Lawrence Livermore National Laboratory. The Advanced Light Source is supported by the Director, Office of Science, Office of Basic Energy Sciences, Materials Sciences Division, of the U.S. Depart-

- [1] P. S. Salmon, *J. Phys. F* **18**, 2345 (1988).
- [2] V. Petkov, S. Takeda, Y. Waseda, and K. Sugiyama, *J. Non-Cryst. Solids* **168**, 97 (1994).
- [3] B. C. Larson, C. W. White, T. S. Noggle, J. F. Barhorst, and D. M. Mills, *Appl. Phys. Lett.* **42**, 282 (1983).
- [4] I. Štich, R. Car, and M. Parrinello, *Phys. Rev. Lett.* **63**, 2240 (1989).
- [5] Y. Waseda and K. Suzuki, *Z. Phys. B* **20**, 339 (1975).
- [6] J. P. Gabathuler and S. Steeb, *Z. Naturforsch A* **34**, 1314 (1979).
- [7] K. Murakami, H. C. Gerritsen, H. van Brug, F. Bijkerk, F. W. Saris, and M. J. van der Wiel, *Phys. Rev. Lett.* **56**, 655 (1986).
- [8] H. C. Gerritsen, H. van Brug, F. Bijkerk, K. Murakami, and M. J. van der Wiel, *J. Appl. Phys.* **60**, 1774 (1986).
- [9] Z. Chang, A. Rundquist, J. Zhou, M. M. Murnane, H. C. Kapteyn, X. Liu, B. Shan, J. Liu, L. Niu, M. Gong, et al., *Appl. Phys. Lett.* **69**, 133 (1996).
- [10] F. C. Brown and O. P. Rustigi, *Phys. Rev. Lett.* **28**, 497 (1972).
- [11] F. C. Brown, R. Z. Bachrach, and M. Skibowski, *Phys. Rev. B* **15**, 4781 (1977).
- [12] K. Sokolowski-Tinten, J. Bialkowski, A. Cavalleri, and D. von der Linde, *Phys. Rev. Lett.* **81**, 224 (1998).
- [13] S. I. Anisimov, N. A. Inogamov, A. M. Oparin, B. Rethfeld, T. Yabe, M. Ogawa, and V. E. Fortov, *Appl. Phys. A* **69**, 617 (1999).
- [14] M. C. Downer and C. V. Shank, *Phys. Rev. Lett.* **56**, 761 (1986).
- [15] A. Miotello and R. Kelly, *Appl. Phys. A* **69**, S67 (1999).
- [16] H. W. K. Tom, G. D. Aumiller, and C. H. Brito-Cruz, *Phys. Rev. Lett.* **60**, 1438 (1988).
- [17] A. L. Ankudinov, B. Ravel, J. J. Rehr, and S. D. Conradson, *Phys. Rev. B* **58**, 7565 (1998).
- [18] H. O. Jeschke, M. E. Garcia, and K. H. Bennemann, *Phys. Rev. Lett.* **87**, 15003 (2001).
- [19] H. O. Jeschke, M. E. Garcia, M. Lenzner, J. Bonse, J. Krueger, and W. Kautek, *Appl. Surf. Sci.* **197-198**, 839 (2002).
- [20] I. Kwon, R. Biswas, C. Z. Wang, K. M. Ho, and C. M. Soukoulis, *Phys. Rev. B* **49**, 7242

- (1994).
- [21] A. I. Nesvizhskii and J. J. Rehr, *J. Synchrotron Radiat.* **6**, 696 (1999).
 - [22] A. L. Ankudinov, A. I. Nesvizhskii, and J. J. Rehr, *Phys. Rev. B* **67**, 115120 (2003).
 - [23] G. T. Barkema and N. Mousseau, *Phys. Rev. Lett.* **62**, 4985 (2000).
 - [24] K. Laaziri, S. Kycia, S. Roorda, M. Chicoine, J. L. Robertson, J. Wang, and S. C. Moss, *Phys. Rev. B* **60**, 13520 (1999).
 - [25] J. J. Rehr and R. C. Albers, *Rev. Mod. Phys.* **72**, 621 (2000).
 - [26] R. Buczko, G. Duscher, S. J. Pennycook, and S. T. Pantelides, *Phys. Rev. Lett.* **85**, 2168 (2000).
 - [27] M. M. Martynyuk, *Sov. Phys. Tech. Phys.* **19**, 793 (1974).
 - [28] The disappearance in EXAFS oscillations past the L_I edge was confirmed by a phase-corrected fast-fourier transform of the data which shows that the laser heating suppresses the nearest-neighbor peak of solid Si to below the noise level.
 - [29] Note also that, due to uncertainties in the assumed areal density of the foils, the plotted absolute cross section of the 1000 Å foil is $\sim 10\%$ higher than that of the 500 Å foils.
 - [30] In particular, we did not observe any significant edge shift of either the $L_{II,III}$ or L_I edges when turning on final state relaxation.
 - [31] An experimental shift of 4 ± 2 eV was estimated by using the model curves as a guide to the shape of the absorption, performing small contractions and dilations of the underlying structure as a fitting parameter. This procedure is also how we estimate the error in the change of the nearest-neighbor distance.

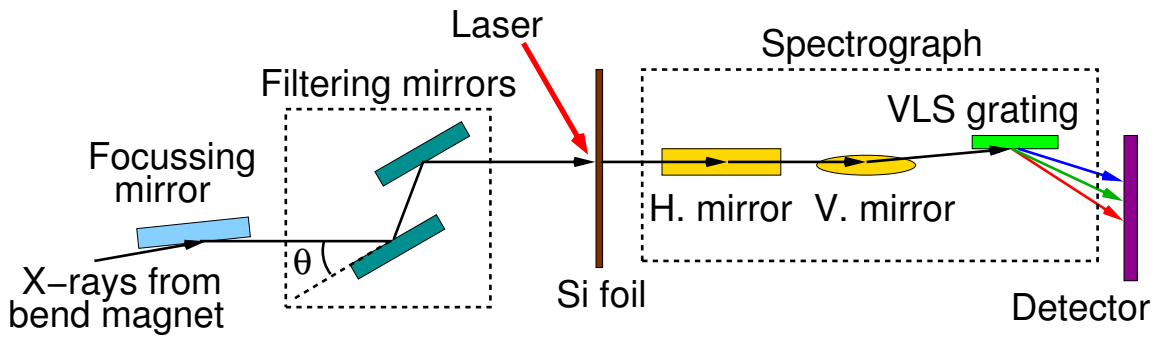


FIG. 1: Sketch of setup at ALS beamline 5.3.1.

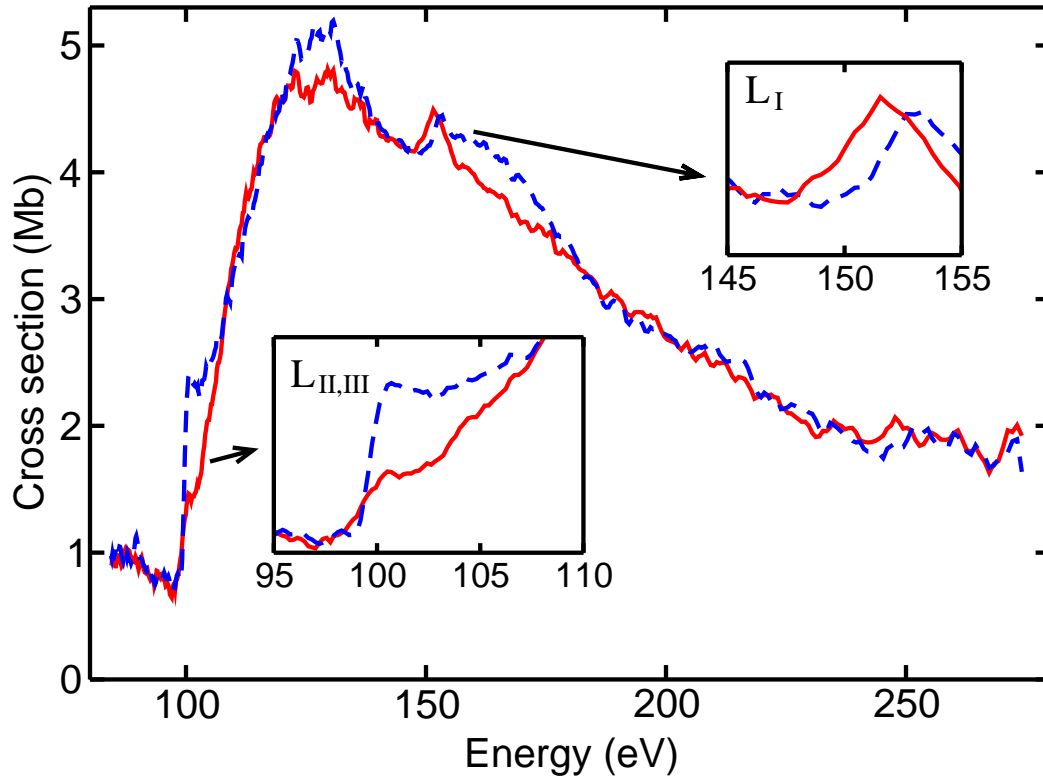


FIG. 2: Absorption spectra of the 500 Å foils before (dashed curve) and 100 ps after (solid curve) laser excitation. The plots show the average of about 100 laser/x-ray shots.

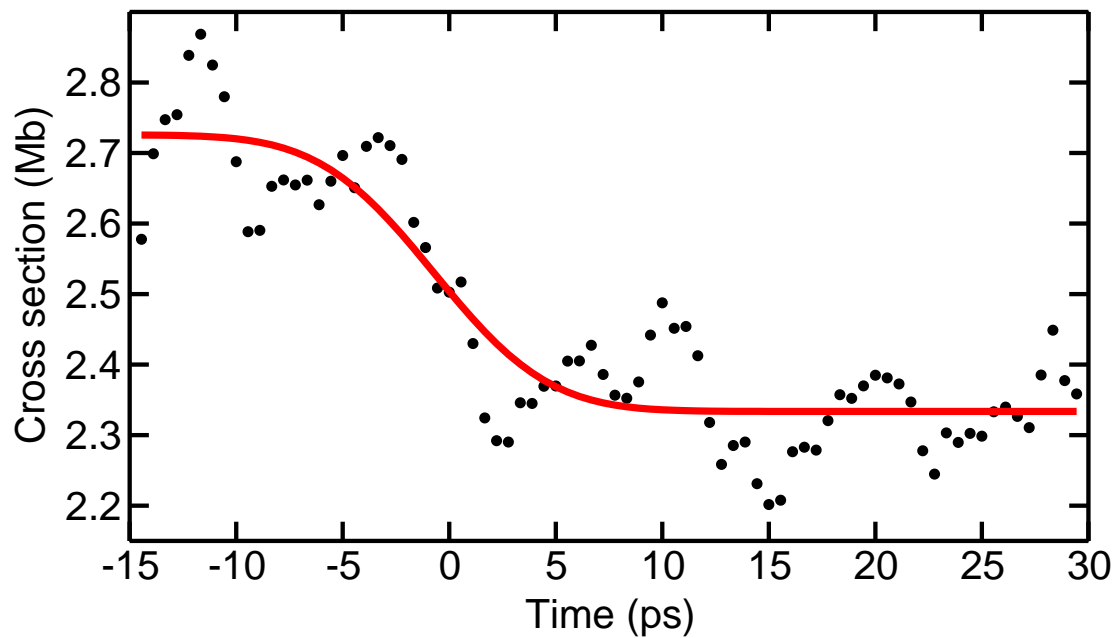


FIG. 3: Absorption of a 1000 Å Si foil immediately above the $L_{\text{II,III}}$ edge as a function of time after laser excitation. The data points show the average of 140 shots. The curve shows a fit of the data to a step function convolved with a 5 ps FWHM gaussian.

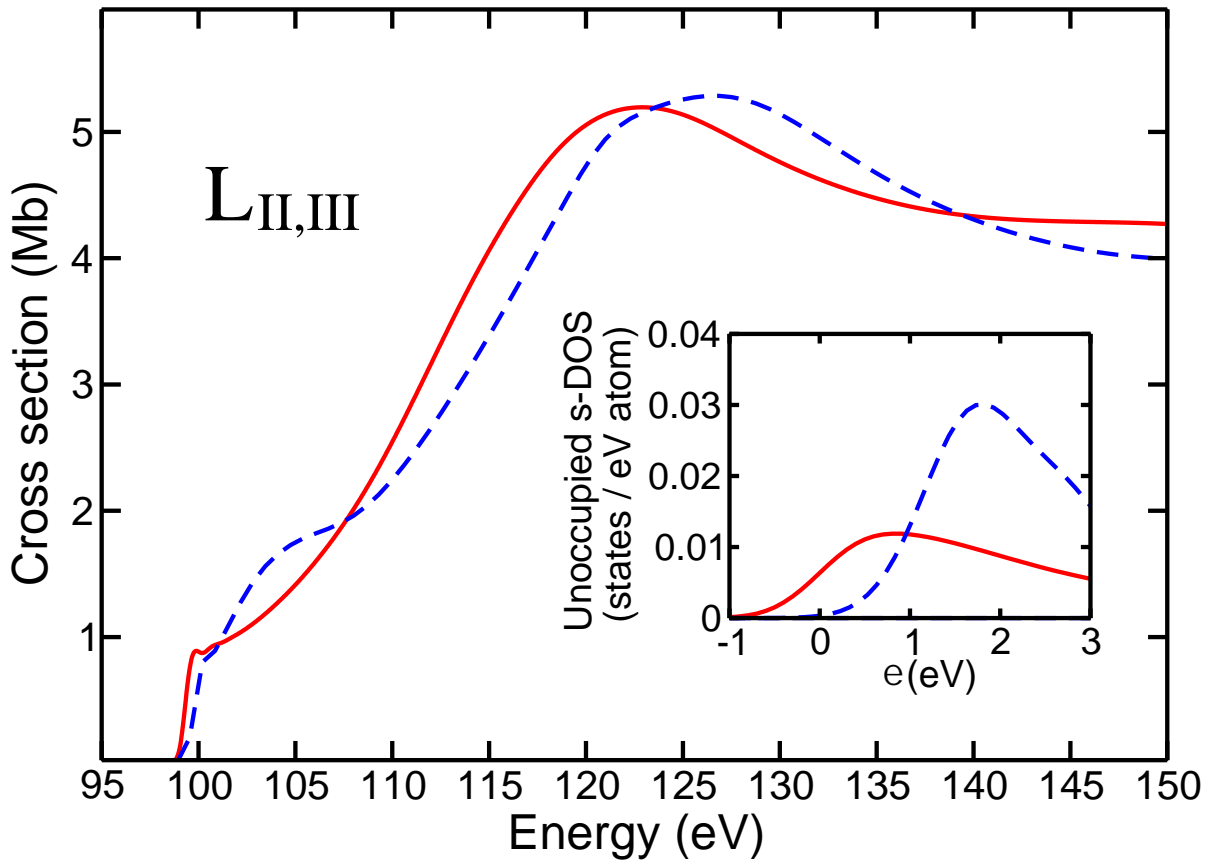


FIG. 4: Comparison of FEFF calculations for liquid Si (solid curve) and the unheated Si (dashed curve) near the $L_{II,III}$ edge. The inset shows the unoccupied 3s-projected density of states as calculated by the MD simulations, convolved with a 1 eV FWHM gaussian to approximate experimental resolution at the edge. The zero of the electron energy ϵ is set to the calculated Fermi level of the liquid.

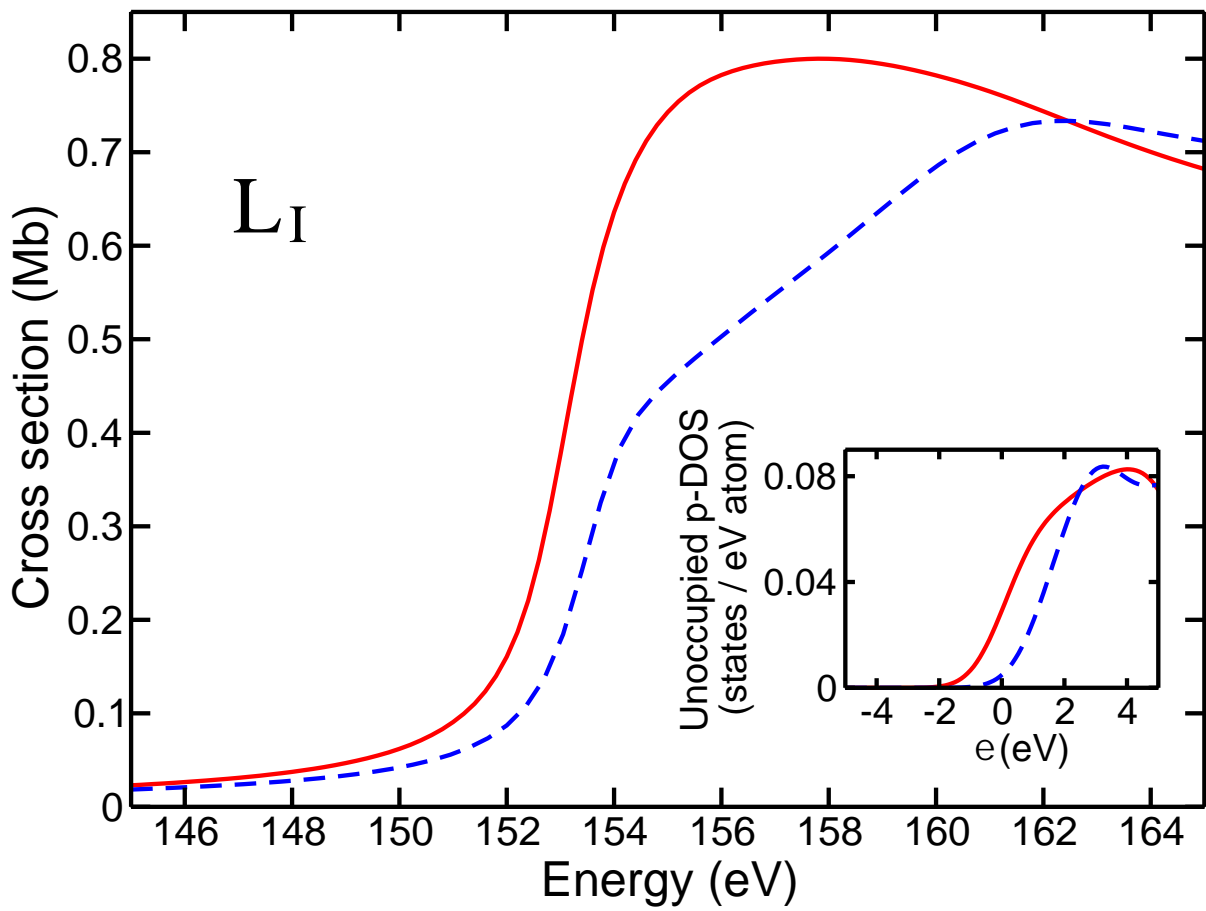


FIG. 5: Comparison of FEFF calculations for liquid Si (solid curve) and the unheated Si (dashed curve) near the L_I edge. The inset shows the unoccupied 3p-projected density of states from the MD simulations, convolved with a 2 eV FWHM gaussian.